Key Engineering Materials
ISSN: 1662-9795, Vol. 926, pp 1850-1863
doi:10.4028/p-1zcpjl

Submitted: 2021-12-09
Revised: 2022-01-31
Accepted: 2022-02-02
Online: 2022-07-22

Rapid Heat Control for Thermoplastic Injection Tooling Using Lattice Structures as Heat Exchanger

Arthur Lepoivre[1,a], Denis Edelin[1,2,b*], Nicolas Baudin[1,c], Jérôme Soto[1,2,d], Maxime Villière[1,3,e], Benoît Redais[4,f], Didier Delaunay[1,g], Vincent Sobotka[1,h]

[1]Université de Nantes, CNRS, LTeN, 44000 Nantes, France

[2]Icam ouest, 44470 Carquefou, France

[3]Capacités S.A.S., 44200 Nantes, France

[4]CERO, 85300 Challans, France

[a]arthur.lepoivre@univ-nantes.fr, [b]denis.edelin@univ-nantes.fr, [c]nicolas.baudin@univ-nantes.fr, [d]jerome.soto@icam.fr, [e]maxime.villiere@capacites.fr, [f]b-redais@cero.fr, [g]didier.delaunay@univ-nantes.fr, [h]vincent.sobotka@univ-nantes.fr

Keywords: injection molding, lattice structure, heat transfer coefficient, aspect quality, RHCM.

Abstract. Since conventional cooling systems with channels are not adequate to achieve a high appearance quality with a short cycle time, a better concept has to be used to control the fast variation of temperature in the mold, close to the injected part. Recently, with advanced manufacturing technologies like 3D-printing, rapid heat cycle molding are developing, using for example lattice structures as heat exchanger inside the mold. Our work proposes an experimental study to analyze the influence of four lattice structures that were specifically designed for this industrial application. An instrumented bench was developed at the laboratory scale, to test the thermal efficiency of the lattice. The material and geometry of the lattice structures were selected based on their thermomechanical properties and their efficiency as a heat-exchanger. The instrumentation of the bench consists in measuring the flow rate and the pressures in the fluid, and also the temperatures at various locations. This allows us to determine the performances of the lattice structure. The results show that the denser the lattice structure, the better, whether considering the mechanical resistance or the thermohydraulic performances. The key element to understand this phenomenon is the average velocity of the fluid flowing inside the lattice structure, accelerating when the porosity decreases and thus bringing a more intense heat exchange.

Introduction

One of the current challenges of the thermoplastic injection industry is to have a high-speed molding process while preserving a high quality aspect. Among the main parameters influencing the morphology of the part, the mold temperature management is important [1].

Conventional injection cooling is performed with channels, directly machined within the injection tool, where a coolant (mainly water, oil or steam) is flowing. These channels need to be far enough from the surface of the polymer to ensure a thermal homogeneity and thus avoid any thermal marking of the part.

During the filling of the mold, the molten polymer undergoes a high cooling rate when contacting the surface of the mold, instantly freezing on the edges close to the mold, as shown in Fig. 1. The polymer that remains molten continues to flow in the middle. These two phenomena create a structure called skin-core [1]. Because of the high cooling rate, the viscosity rises quickly and the polymer undergoes high shear stress, causing visible defects on the part such as flow marks [1]–[3], which are not wanted with the automotive standards.

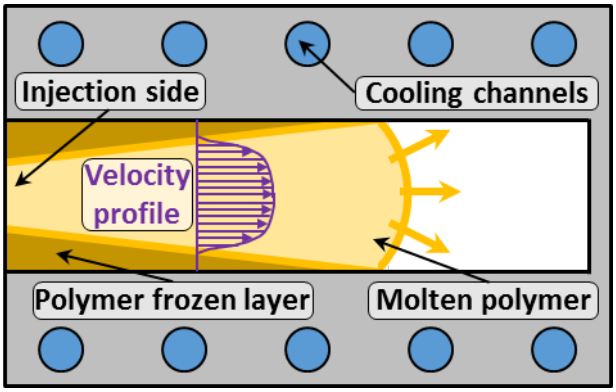

Fig. 1– Phenomena during the injection of the polymer in conventional cooling, inspired from [4].

With conventional cooling, the temperature control of the surface mold is slow because of the thermal diffusivity of the mold material and the distance between the channels and the mold cavity. Rapid heat cycle molding (RHCM) is a solution for the manufacturers, by heating and cooling the mold faster and therefore improving the surface quality of the injected parts [5], with an acceptable cycle time. The surface of the mold needs to be heated enough, usually above the glass transition temperature, before the injection, to ensure a lower thermal shock between the melted polymer and the mold [5]. Then the mold is quickly cooled at a sufficient temperature to reach a lower viscosity for the polymer, and to eject the molded part without warping it. A lot of solutions can be implemented, generally organized with two strategies. The first one is to work with a mold with low thermal mass, using materials with low density, low specific heat, small volumes, porous materials or insulated multilayer structures [4]. The second strategy is to use rapid heat method, by electrical resistance, induction, thermoelectricity, convection, radiation or contact [4]. Some of these concepts can also be combined.

Tian *et al.* [6] proposed a study about heat dissipation medium made of a cellular repetitive pattern, and compare it with other solutions from the literature. They mention that a diamond-shaped structure is better for the heat exchange, with better performances when the conduction through the ligaments is facilitated by a continuity of the material. Their solution seems superior to other concepts, such as channels, louvered fins, corrugated ducts, packed bed, metallic foams and some lattice-frame materials.

Previous authors studied mostly numerically the influence of metallic foam [5], [7], [8] or lattice structure [9] for the same industrial application about injection molds, but with limited experimental thermal studies, performed with only one or two thermocouples depending on the cited studies.

To gain the same benefits as the other RHCM solutions, the objective of this work is to use a lattice structure as a heat-exchanger to accelerate the temperature variation of the mold surface, and prevent the apparition of visual defects. Through an experimental approach, we aim to describe the coupled heat transfer and hydraulic phenomena during cooling and heating phases. We first explained the design methodology for the lattice structure that has to meet several criteria such as mechanical resistance and thermo-hydraulic performances. Then, we developed an instrumented bench, at the laboratory scale, to compare the performances of different 3D-printed lattice structures. Finally, we calculated the heat transfer coefficient in quasi-steady state for the different lattice structures, depending on the morphology parameters. Another study was performed in cyclic condition to understand the consequences it has on the temperature evolution at various locations.

1. Methodology

As shown in Fig. 2 (a), an injection mold was adapted to add the lattice structures inside the core block. The mold cavity allows the injection of two 190×55×2 mm^3 thin plates. The goal is to achieve a good appearance quality for the injected part. In order to compare the performances of the solution,

two lattice structures can be inserted inside the core block, as visible in Fig. 2 (b). The global dimensions of the lattice structures are 200×65×30 mm^3, slightly bigger than the injected part.

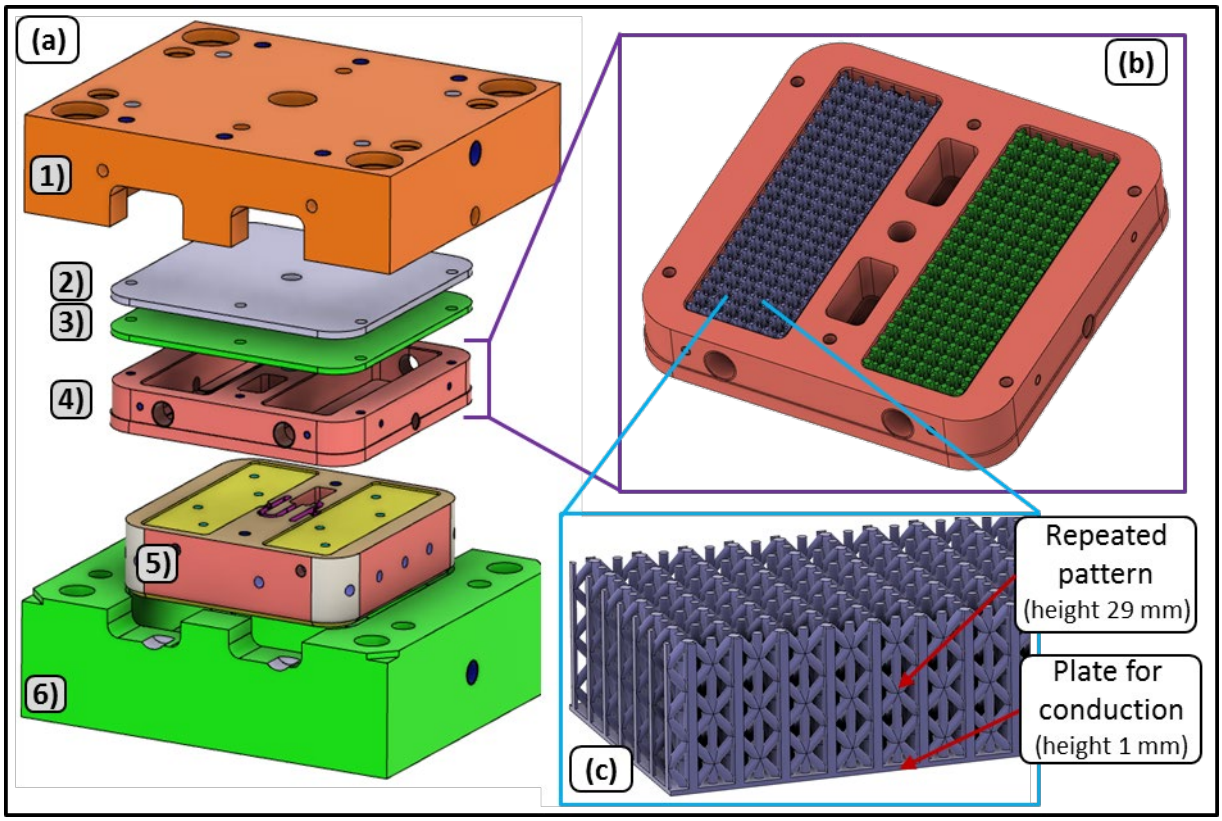

Fig. 2 – Representation of the injection mold with (a) the different elements: 1) the stationary plate, 2) an added insulated plate, 3) an added sealing plate, 4) the core block, 5) the cavity block and 6) the movable plate ; (b) the core block containing two lattice structures and (c) with a zoom on one of the lattice structures.

Lattice structure design

The lattice structures were designed to meet several criteria:

- Mechanical resistance: the structures have to withstand the injection pressure, set to 500 bar in the cavity.
- Hydraulic performances: the pressure drop inherent to the structure needs to be minimal.
- Thermal performances: the heat exchange between the coolant and the lattice structures has to be maximized.

In order to choose the material for the lattice structures, an Ashby chart, plotted in Fig. 3, was used. It shows the best options supposed to be positioned in the top-right corner. Indeed, the compressive strength needs to be high enough, with the minimum value of 1 GPa, based on the mechanical numerical study results presented later with Table 3. Moreover, the material should be highly conductive, with a low thermal inertia, which would give it the highest thermal diffusivity possible. The best options presented in the chart are the Tungsten and Molybdenum, but these materials are too expensive, among other reasons, to consider for industrial use. After, Cu-Be alloys present interesting properties, but are not available with 3D-printing processes. It appears that the steel family is the fourth best option, and was chosen for this application.

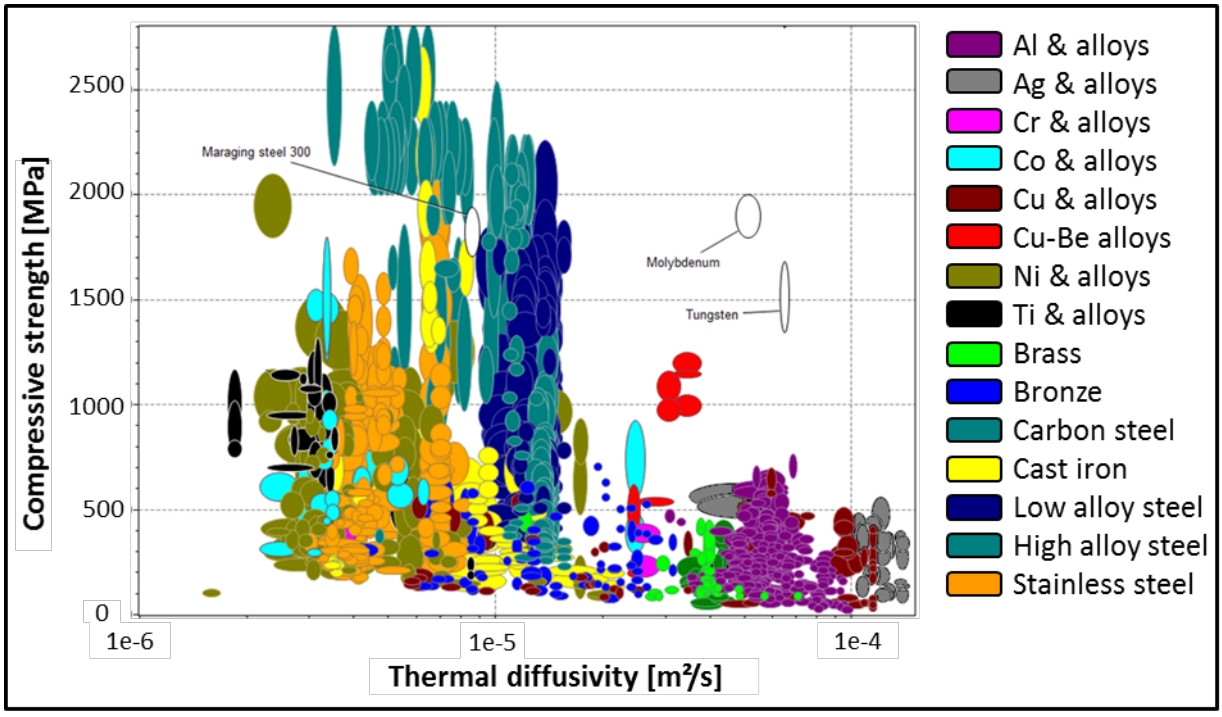

Fig. 3 – Materials cartography obtained with Granta EduPack® software, considering mechanical properties versus thermal diffusivity, with log/linear scale.

The lattice structures were also designed to maximize the heat exchange between the coolant and the mold. Inspired from the literature [6], a diamond-shaped structure was chosen, as it favors the conduction exchange in the vertical direction while it keeps an important exchange surface with the coolant. To manufacture lattice structures with a reasonable cost, metal 3D-printing appeared to be a good solution, and SLM process was chosen among different possibilities. However, the SLM process with our geometry imposes maximum overhang angles of 45° for the cylinders forming the diamond structure, to avoid any printing supports.

As presented in Fig. 4, several configurations were chosen for the lattice structures design, by varying the cylinders diameter, D_c, from 1.5 to 3.0 mm, and the pattern unit size, L_{unit}, from $10\times10\times10$ mm^3 to $15\times15\times15$ mm^3. The influence of the equivalent porosity can be tested by comparing lattices A, B and D. The effect of the pattern units' dimensions are analyzed by studying lattices B and D. Also, a 1-mm-thick thin plate was added in the design at the bottom, with the continuity of the bulk material, to avoid the thermal contact resistances that would occur if all the cylinders were in contact with the mold's core block. Some vertical pillars were also added, to increase the mechanical resistance.

Among the different materials that were available with 3D-printing, maraging steel MS1, also called 1.2709 steel, was chosen from EOS® supplier for its superior mechanical properties. The physical properties are given in Table 1. For more convenience, and to avoid possible defects due to shrinkage, the printed parts remained without age hardening.

Table 1 – Maraging steel MS1 properties. Z direction refers to the vertical printing direction [10].

Physical property	Maraging steel without age hardening	Maraging steel with age hardening
Density [kg/m^3]	8050 ± 50	8050 ± 50
Thermal conductivity [W/(m·K)]	15 ± 0.8	20 ± 1
Specific heat [J/(kg·K)]	450 ± 20	450 ± 20
Yield strength $R_{p0.2\%}$ (Z direction) [MPa]	1000 ± 100	1990 ± 100
Modulus of elasticity (Z direction) [GPa]	150 ± 20	180 ± 20

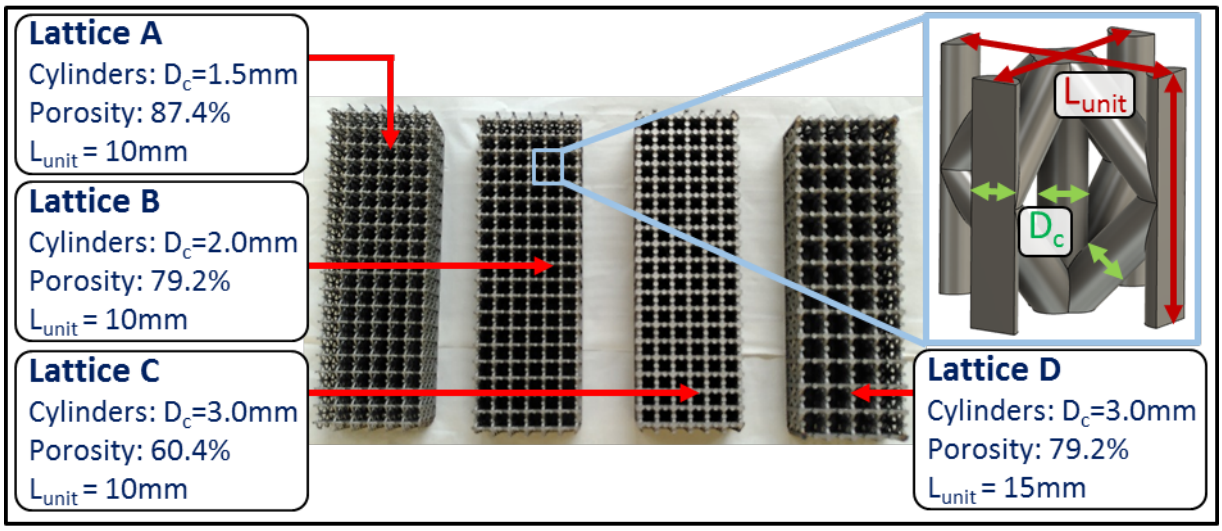

Fig. 4 – Parameters of the lattice structures, with an example of the pattern unit from lattice B.

Mechanical model

The injection mold must not be deformed, to ensure the production of parts with the correct dimensions. The lattice structures being inserted in the core block, next to the molding cavity, it needs to withstand the injection pressure, considered at a maximum of 500 bar for specific polymers. A simple mechanical model was used to check the mechanical resistance of the core block with the designed lattice structures, without exceeding the elastic limit $R_{p0.2\%}$ of the materials, and with a maximum vertical displacement of 0.1 mm.

As shown in Fig. 5 (a), the reduced geometry is made of six repetitive units (in blue), with the core block between the lattice and the injected part (at the bottom, in red) and the sealing plate (at the top, also in red). The boundaries conditions, shown in Fig. 5 (b), are the following: (i) the upper face is fixed, (ii) a 500 bar pressure is applied on the underside, and (iii) there are symmetries on the edges of the lattice structure, the core block and the sealing plate.

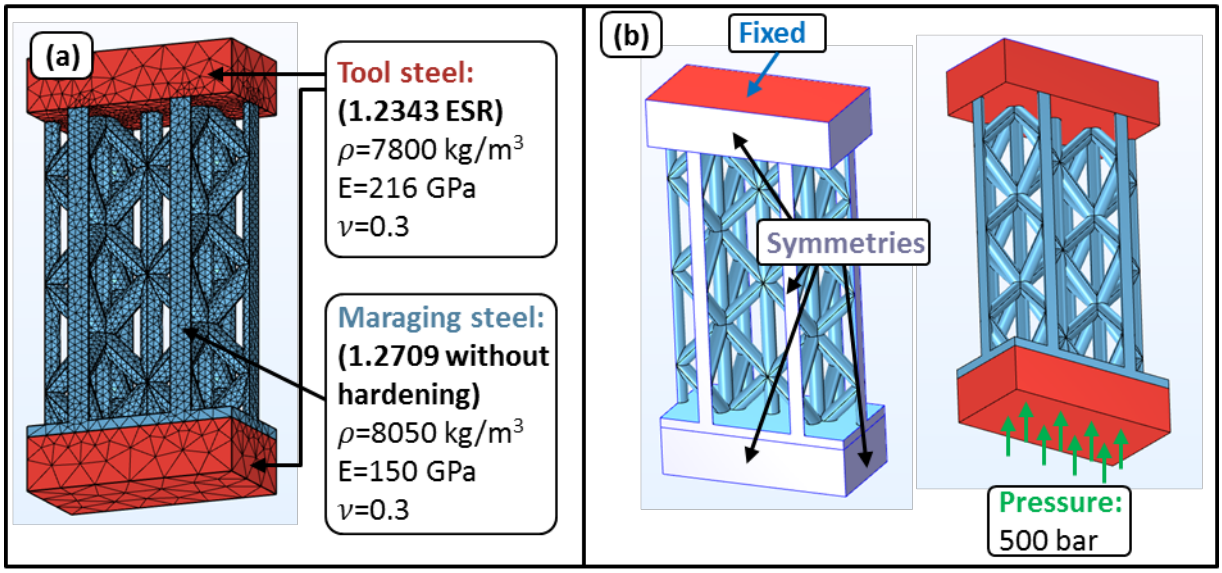

Fig. 5 – Mechanical model description, with (a) the mesh and the materials properties and (b) the boundaries conditions.

A linear elastic model was used, with the properties given in Fig. 5 (a). Numerical solving is done in 3D with COMSOL Multiphysics® v5 in steady state with the built-in solver.

Experimental bench description

From the concept presented in Fig. 2 (a), only elements 2), 3) and 4) were used to build an instrumented bench, at the laboratory scale shown in Fig. 6. Two thermoregulators, with the reference HB-180Z2 from HB-THERM®, one for cold and the other for hot water, were connected to the hydraulic circuit. Six solenoid valves were installed to control the flow of either hot (at 80°C) or cold water (at 25°C), triggered by a switch connected to an Arduino. The hot temperature was imposed by the sensors limitation, and the cold temperature was chosen slightly higher from the one of the distribution water system.

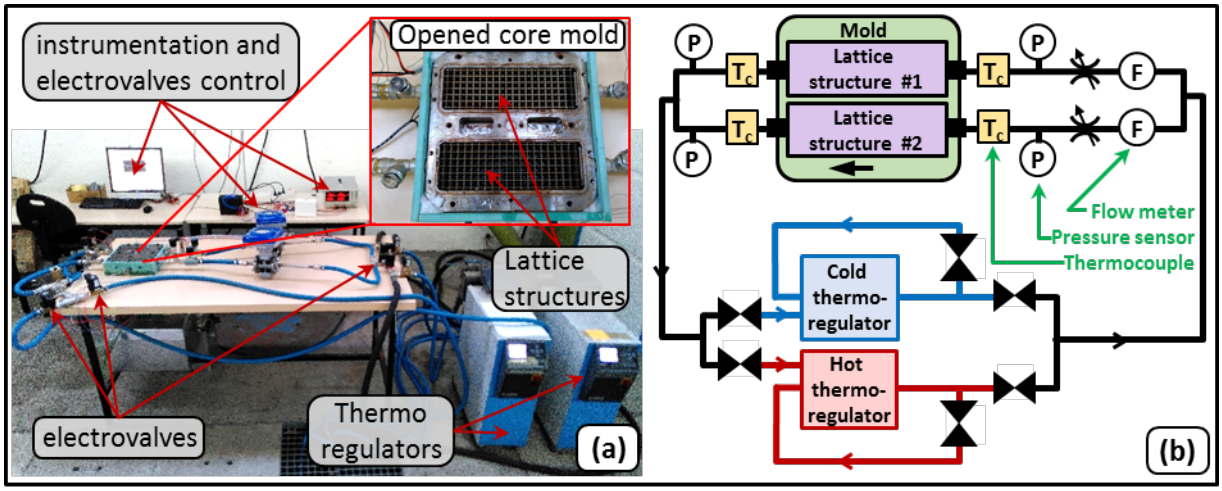

Fig. 6 – (a) Experimental bench description and (b) the associated instrumented hydraulic circuit.

To represent the effects of the injected part and the global physic behavior, a dummy part in PMMA was positioned under the core mold, as shown with Fig. 7, with the same dimensions as the injected part that will be produced with the mold. Insulators were also added all over the core mold.

The hydraulic instrumentation consists in measuring the flow rate and the pressure drop for each of the two channels, as shown in Fig. 6 (b), with in total two electromagnetic flow meters, with the reference OPTIFLUX1050 from KROHNE®, and four absolute pressure sensors, with the reference 3500B from Gems®.

Temperatures are measured with 28 K-type thermocouples in total, at various locations as shown in Fig. 7. For each of the two lattice structures cavities, there are two thermocouples for the inlet (T_{in}) and outlet (T_{out}), three thermocouples inserted in the mold (T_1,T_2,T_3), four thermocouples inserted in the dummy part (T_4,T_5,T_6,T_7) and three thermocouples are placed on an rod (T_8,T_9,T_{10}), inside the wetted cavity. The rod is made of polymer to avoid the axial conduction and was 3D-printed with SLA process. It is placed slightly downstream, to avoid disturbing the measurements at T_2 and T_5. The thermocouples have a metallic sleeve with a total diameter of 1 mm for T_1 to T_7, and 0.5 mm for T_8 to T_{10}.

The acquisitions are performed with a Yokogawa® DL750 for the thermocouples, associated with an external cold box and a PT100 probe. The acquisitions frequencies are equal to 10 Hz for quasi-steady state study, or 50 Hz for the cyclic conditions. The pressure sensors acquisitions are performed with a 16-bit ADC module connected to an Arduino, with a frequency of 2 Hz. The flow rate values are directly read on the sensor.

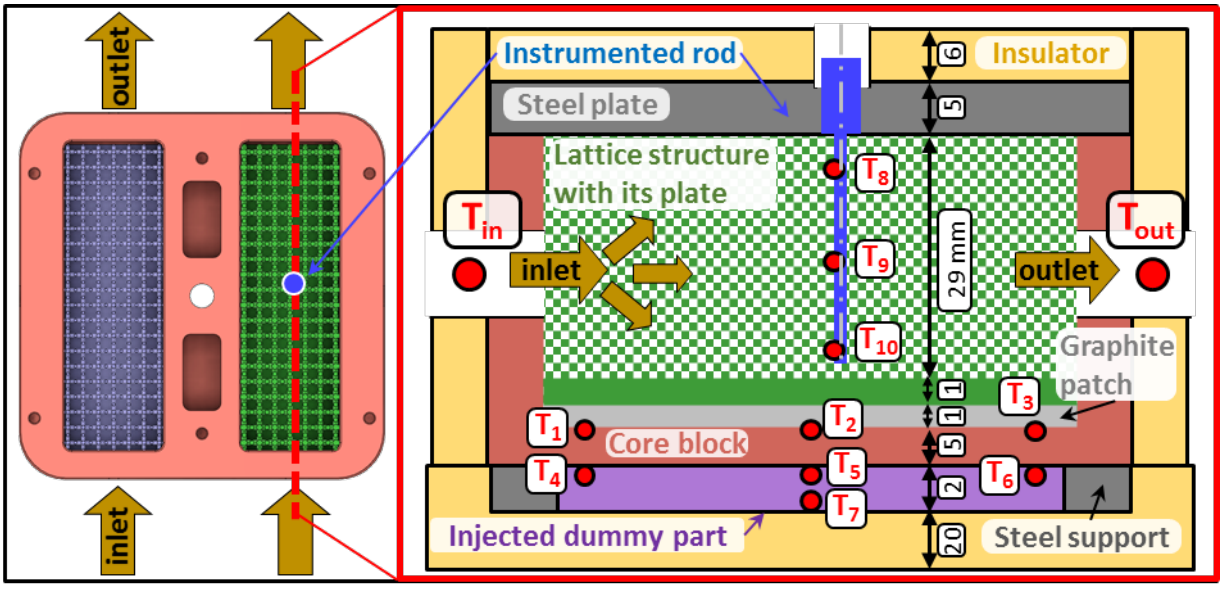

Fig. 7 – Instrumented bench description with thermocouple positions. The scale is not respected on the scheme.

To calculate the exchange performances of the lattice structure during quasi-steady experiments, an equivalent heat transfer coefficient is calculated with

$$h_{eq} = \frac{\dot{m}\, c_p\, (T_{out} - T_{in})}{S\left(T_2 - \left(\frac{T_{inlet}+T_{outlet}}{2}\right)\right)} \quad (1)$$

where $\dot{m}$ is the mass flow rate, c_p is the specific heat, S=0.042 m² is the exchange surface of the coolant with the six surfaces forming the core block cavity, and T is the temperature with the locations specified in Fig. 7.

This coefficient is considered as equivalent because the thermocouple in the core block (T_2) is not directly in contact with the water. Indeed, there is the 1-mm-thick graphite patch and the 1-mm steel plate above. However, this equivalent coefficient is always calculated the same way for the four lattice structures, thus giving comparative information.

2. Results and Discussions

The four lattice structures are tested. First, a mechanical study presents the resistance of the geometries. Then, the thermohydraulic performances are investigated, in terms of heat exchange and pressure drop in quasi-steady state. Lastly, some experiments are performed in cyclic conditions to mimic the industrial process.

Mechanical resistance

The results of the mechanical study are presented in Fig. 8 for lattice C, showing the vertical displacement of the geometry and the Von-Mises stress, with stress concentration located at the cylinders junctions.

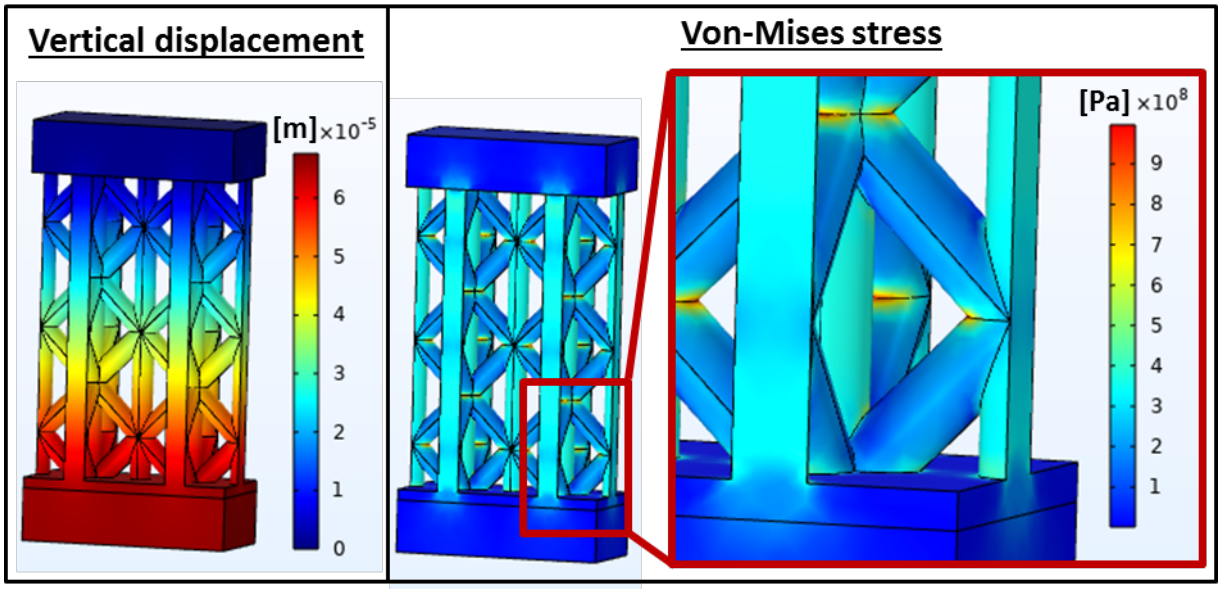

Fig. 8 – Results of the mechanical simulation for lattice C.

The maximum Von-Mises stress and vertical displacement are given in Table 2 for the four lattice structures. The maximum Von-Mises stress is superior to the yield strength ($R_{0.2\%}$=1000 MPa) of the maraging steel for lattices A and D. Thus, lattice structures A and D require the heat treatment for maraging steel [10], to increase the yield strength ($R_{0.2\%}$=1990 MPa). Another possibility is to reduce the injection pressure below 500 bar, an overestimated value to ensure a security factor.

Table 2 – Mechanical results for the four lattice structures. The vertical axis is considered as the same direction of the applied pressure.

	Maximum Von-Mises stress [MPa]	Without age-hardening: maximum vertical displacement [mm]	With age-hardening: maximum vertical displacement [mm]
Lattice A	1760	Yield strength exceed	0.10
Lattice B	997	0.07	0.06
Lattice C	516	0.03	0.03
Lattice D	1210	Yield strength exceed	0.06

The criterion of 0.1 mm for the maximum vertical displacement was required by the industrial partner, to respect the geometrical tolerances of the injected part. All the structures respect this criteria, considering the age-hardening for lattices A and D, and with or without this age-hardening for lattices B and C.

As expected, with the diameter increasing, the structure becomes more resistant, as found by comparing lattices A, B and C. Likewise, a small pattern unit size L_{unit} (see Fig. 4) is preferred to increase the mechanical resistance (comparison of lattice structures C and D, for the same cylinder diameter D_c=3 mm).

For structures such as lattice C, the maximum Von-Mises stress is low enough to imagine another material choice for the structure, less resistant, but with better thermal properties. For example, with a maximum compression resistance of 500 MPa, the material cartography shown in Fig. 3 indicates that some aluminums would be better candidates than the steel we use, with a thermal diffusivity of 6.0×10^{-5} m²/s instead of 4.4×10^{-6} m²/s for the chosen maraging steel, thus increasing with a factor of 14.

Pressure drop

The pressure drops on the four structures measured with the sensors are presented in Table 3, depending on the flow rate Q.

Table 3 – Pressure drop results, depending on the flow rate Q considered in [m^3/s].

	Pressure drop [Pa]	Associated correlation coefficient
Lattice A	$1.09 \cdot 10^{10}\ Q^2 + 2.11 \cdot 10^7\ Q$	$R^2=0.71$
Lattice B	$1.13 \cdot 10^7\ Q^2 + 2.66 \cdot 10^7\ Q$	$R^2=0.96$
Lattice C	$5.41 \cdot 10^{11}\ Q^2 + 6.00 \cdot 10^7\ Q$	$R^2=0.98$
Lattice D	$3.58 \cdot 10^9\ Q^2 + 2.52 \cdot 10^7\ Q$	$R^2=0.92$

The pressure drop versus flow rate of lattices A, B and D are globally the same, with only 22% variation between the minimum and the maximum. Lattice C has a pressure drop 5 times higher than the average of the other three. For lattice C with a flow rate of 10.4 L/min, the pressure drop is 0.285 bar, on a length of 200 mm, thus corresponding to a hydraulic gradient of 1.42 bar/m. This pressure drop is negligible, compared to the pipes and junctions of the experimental bench, with pressure values between 3 and 4 bar when there is no lattice structure inserted in the mold. With those pressure drop values, the industrial thermoregulator pumps are still able to deliver enough power.

Thermohydraulic performances

The temperature evolution versus time are given in Fig. 9, in heating conditions, with the thermocouples locations already described with Fig. 7.

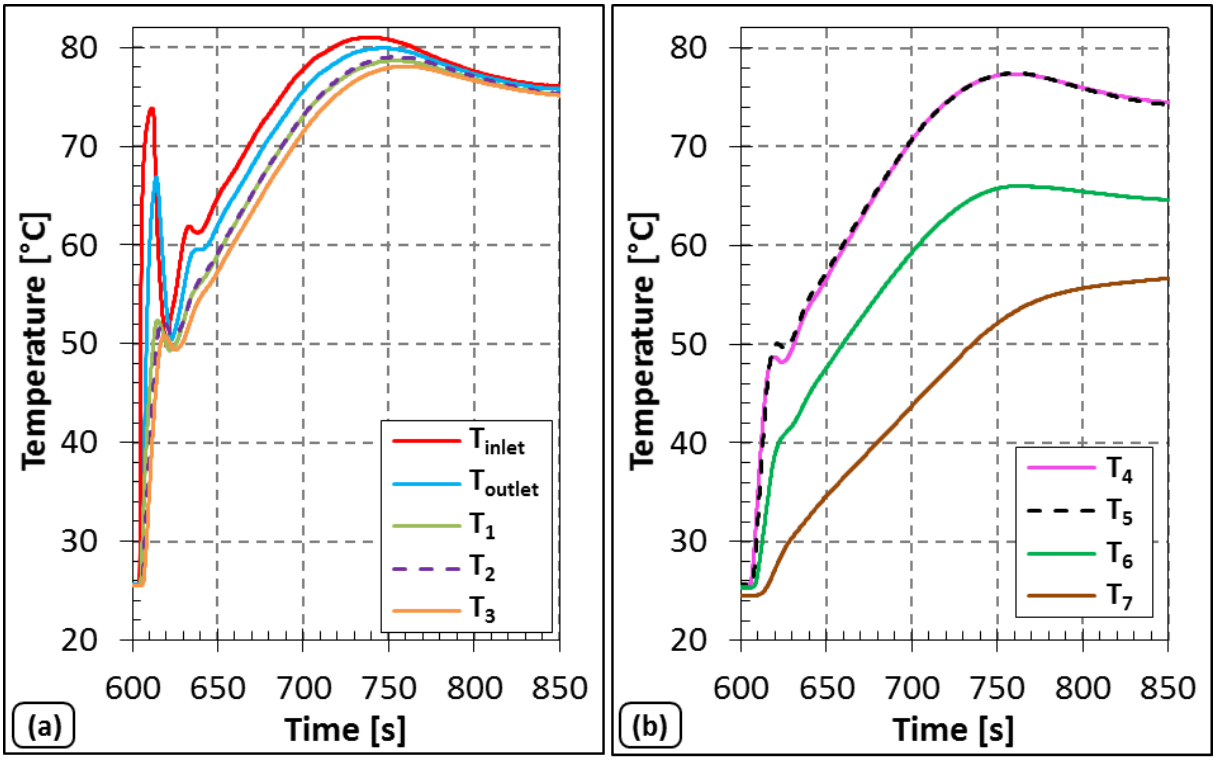

Fig. 9 – Temperatures evolution versus time, for lattice C in heating with 8.9 L/min.

At the beginning, a temperature peak is visible on the inlet and outlet temperatures. The increase corresponds to the hot water entering the mold and the decrease to an unwanted situation: the cold water that was in the mold and the pipes previously, representing 2.0 L, is going back into the thermoregulator within the closed circuit. The thermoregulator, with a tank capacity of 2.1 L, does not have the time to heat the water enough, which is then injected again in the mold. A supplementary supply tank, or a better thermoregulator, would be required to avoid this situation.

As expected, the temperatures inside the core block, T_1, T_2 and T_3 in Fig. 9 (a), are directly linked to the variation of the inlet temperature T_{inlet}, with a delay time. The same goes for T_4 and T_5, the upstream and middle temperatures inside the dummy part, that present the same trend, with a longer delay. The downstream temperature, T_6, is colder by around 10°C for the example presented in Fig. 9 (b). Because T_4 and T_6 are placed in a symmetric way, we suppose there is a problem with the thermal grease spreading, between the core block and the dummy part, thus causing a much slower heat exchange. The colder temperature of T_6 can also be explained by a possible dead zone flow in the upstream area of the lattice structure, because T_3 is inferior to T_1 and T_2. The temperature under the dummy plate, T_7, is also slower to equilibrate, because of the thermal diffusivity of the polymer, with a thickness of 2 mm. Moreover, this temperature gap effect is not visible with the difference of T_{inlet} and T_{outlet}, which means that this thermal heterogeneity is limited to the area close to T_6.

The temperatures of the instrumented rod (T_8,T_9,T_{10}) are very homogenous. For example, for lattice C in heating at 8.9 L/min, the average of the standard deviations for each time step is equal to 0.02 °C. The other lattice structures present the same tendency. This means that there is a very low temperature gradient in the water, in the height of the lattice structure.

To test the thermohydraulic performances of the four lattice structures, a total of 56 experiments were performed, with different flow rates. The results are shown in Fig. 10, with the equivalent exchange coefficient from Eq. (*1*), in quasi-steady state, versus (a) the flow rate in L/min, and (b) the average speed in m/s. The average speed is calculated by dividing the flow rate by the thinnest cross section area of the lattice structures, thus with the sum of the triangle shaped holes' area. The results are shown in heating conditions from 25°C to 80°C, represented with squares, and in cooling conditions from 80°C to 25°C with diamonds. In Fig. 10 (b), the equivalent Reynolds and Nusselt scales are given, proportional to the average velocity and the heat transfer equivalent coefficient. The characteristic length taken into account in this situation is the height of the lattice structures, equal to 0.03 m.

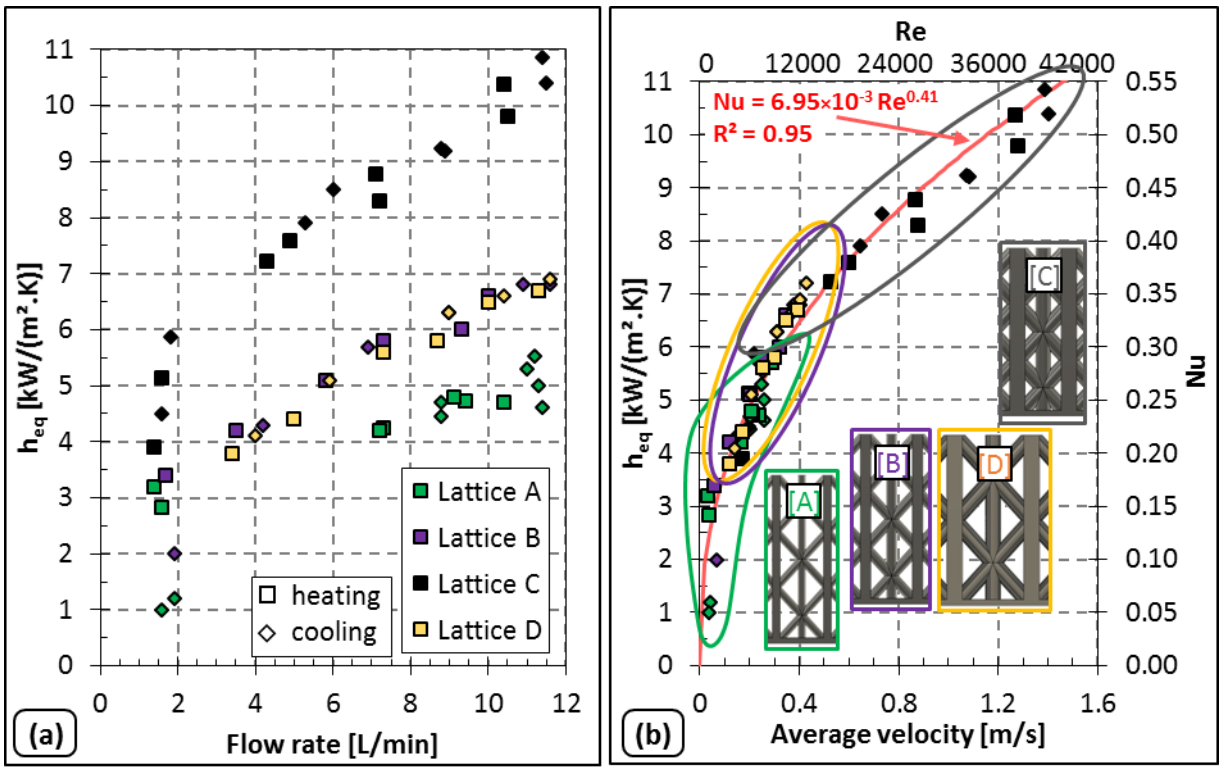

Fig. 10 – Thermohydraulic performances in quasi-stationary state.

The results from Fig. 10 (a) show a hierarchy in terms of performances between the four lattice structures, with lattice C being the best, lattices B and D equivalently medium, and lattice A being

the worst. Repeatability is verified, with multiple tests for the same flow rate, and by exchanging the lattice structure position between the two cavities in the core block. Performances in heating conditions appear to be the same as the ones in cooling conditions.

First, by comparing the pattern unit size L_{unit} at iso-porosities (lattices B and D), there is no difference on the performances. If a choice must be made between these two structures, lattice B could be chosen, but only by considering its higher mechanical resistance, as presented earlier with Table 2.

Secondly, the most interesting results are about the cylinder diameter influence, by comparing lattices A, B and C. When the diameter of the cylinders increases from D_c=1.5 mm (lattice A) to 3 mm (lattice C), h_{eq} values are multiplied by 2. This result was not expected, as we assumed that the equivalent heat transfer coefficient would rise with porosity level increase.

To explain this phenomenon, Fig. 10 (b) shows the same equivalent coefficient, but this time plotted versus local velocity, more representative of the water convection intensity. All the lattice structures performances follow the same shape. A power law curve

$$Nu = 6.95 \cdot 10^{-3} \times Re^{0.41} \quad (2)$$

was fitted on 50 experimental points, with a correlation coefficient of R^2=0.95. This fit did not consider the 6 experiments that were below 0.1 m/s, equivalent to Re=3000, with a possible different fluid dynamic effect. Moreover, these data correspond to a very low flow rate (1.4 to 1.9 L/min), highly inferior to the flow rates targeted in our industrial context, where we want it to be maximized.

Unfortunately, this equivalent heat transfer coefficient is not comparable with the other values that could be found in the literature, because of the way it is calculated, as explained with Eq. (*1*) details.

The contact surface of all the lattices with the bottom plate, S1, and with the cylinder forming the heat exchanger, S2, are given in Table 4. From the convective heat exchange with the water, S1 is relative to the direct exchange with the flat plate, and S2 is linked to the conductive heat exchange along the steel cylindrical pillars. Because of the repartition of S1 compared to S2 that is globally the same, with S1 representing 5% to 10% of the total exchange surface, it is difficult to conclude on a predominant effect that would come from either the bottom flat plate, or from the cylinders' conductive effects.

Table 4 – Exchange area repartition between the flat plate and the cylinders.

	S1: exchange area with the bottom plate without the cylinders [m²]	S2: exchange area with the cylinders only [m²]	S1 + S2 [%]
Lattice A	0.011	0.118	8.7% + 91.3%
Lattice B	0.010	0.138	7.0% + 93.0%
Lattice C	0.008	0.147	5.1% + 94.9%
Lattice D	0.011	0.095	10.0% + 90.0%

Among all the lattice structures, the best geometry is the one with the lower passage section, lattice C. A more intense convection exchange happens, that is made with the contact of (i) the flat plate at the bottom of the lattice structure, and (ii) of all the cylinders forming the lattice structure.

Thermohydraulic performances under cyclic conditions

The performances are now studied under cyclic conditions, more representative of the industrial injection process. The cycle is composed of a 10-s heating at 80°C, followed by a 25-s cooling at 25°C, for a total cycle of 35 s. These times were selected after several trials, but always with the 35 s total cycle limitation. In total, 12 experiments are performed. For all the lattice structures, three different flow rates are tested, with low (2.9 to 4.0 L/min), medium (8.6 to 8.9 L/min) and high (10.9 to 11.6 L/min) values. The results for lattice C on medium flow rate are presented in Fig. 11.

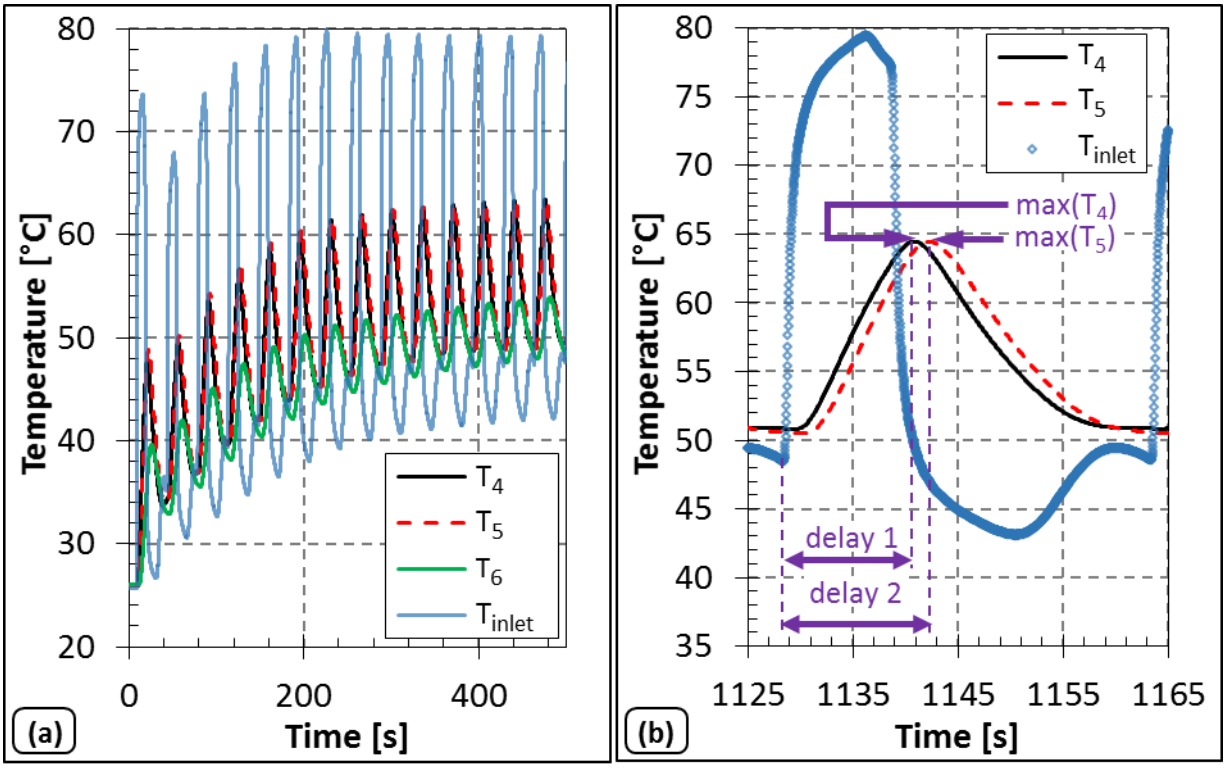

Fig. 11 – Temperatures evolutions for lattice C with Q=8.8 L/min, given with (a) multiple cycles and (b) a zoom on only one cycle on periodic steady state.

The establishment of the periodic steady state is visible in Fig. 11 (a). The inlet temperature evolution needs 7 cycles to stabilize whereas the dummy part temperatures need between 12 cycles (for T_4 and T_5) and around 30 cycles (for T_6). As explained earlier, T_6 is supposed to be located close to a dead zone flow, causing much slower temperature variation, and is therefore not taken into account for the rest of the study.

Only one cycle is studied, on periodic steady state, shown in Fig. 11 (b). First, it shows the time delays between the beginning of the hot water injection and the peaks of T_4 (delay 1) and T_5 (delay 2). Secondly, the maxima of temperatures reached for the same two peaks, max(T_4) and max(T_5), can be pointed out. These pieces of information are important criteria to consider for the industrial application. For the 12 experiments, these criteria are plotted versus flow rate in Fig. 12.

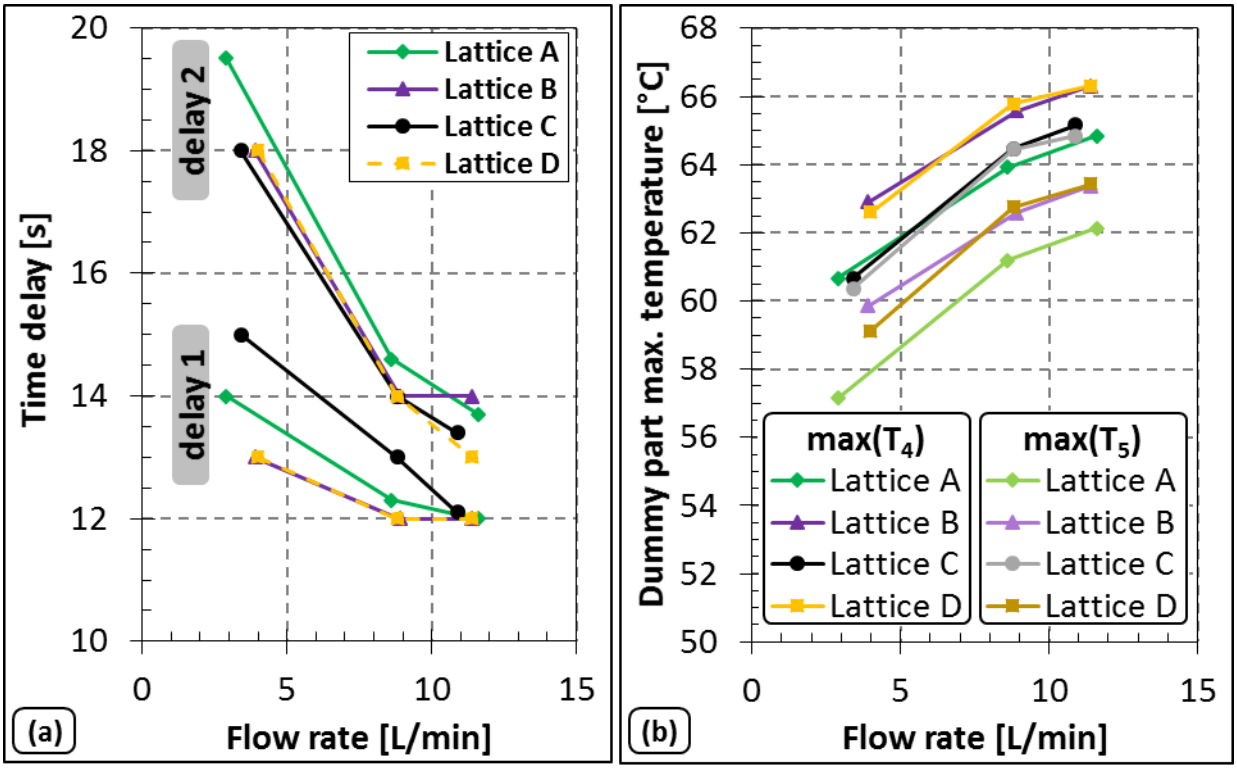

Fig. 12 – Periodic conditions results with (a) the delay between the inlet temperature rise and the dummy part temperature peak and (b) the maximum temperature reached on the peak for T_4 and T_5.

Fig. 12 (a) can be used to know when to trigger the heating, which has to be done before the injection starts to take into account the delay of temperature rise. Also, Fig. 12 (b) can be analyzed to identify the best lattice structure for the cyclic conditions. Lattices B and D present higher maximum temperatures, from 63°C to 66°C for T_4. However, they present also a high heterogeneity, with an average of 3.1°C between max(T_4) and max(T_5). Once again, lattice C appears to be the best structure: with slightly lower maximum peak temperatures on T_4, it has a very good thermal homogeneity, with an average of 0.2°C between max(T_4) and max(T_5).

All the results from the mechanical analysis, the quasi-steady state study and the cyclic situation indicate that lattice C as an insert in a molding tool is the best geometry among the others for rapid heat cycle molding.

3. Conclusions

This study has presented the methodology to use a heat exchanger inside a molding tool, to achieve fast temperature evolution at the surface in contact with the molten polymer. First, the design methodology of the lattice structure was given, with the material choice confirmed by a mechanical study and the geometry selection, inspired from the literature. Then an experimental set-up was developed, with instrumentation to obtain the temperatures, the pressure drops and the flow rates inside the molding tool and the coolant. Finally, the information provided by the sensors were post-processed and analyzed for each lattice structure, for different flow rates, in heating or cooling situations and on quasi-steady state or under cyclic conditions.

The main results of this work indicate lattice C as the best solution. It withstand the injection pressure better, and presents better thermohydraulic performances. This lattice has a denser structure than the others, causing the heat exchange to raise with the increase of the average speed, triggering a more intense convection exchange between the coolant and the mold.

To go further, it would be interesting to develop a numeric tool to predict the heat transfer going on the lattice structure, and the fluid dynamics of the coolant. With such tool, the geometry of the

lattice structure could be optimized to maximize the heat exchanges. Also, other materials could be investigated, as long as the structure is resistant enough to the injection pressure.

References

[1] G. J. Zhong and Z. M. Li, "Injection molding-induced morphology of thermoplastic polymer blends," *Polym. Eng. Sci.*, vol. 45, no. 12, pp. 1655–1665, 2005.

[2] A. M. Grillet, A. C. B. Bogaerds, G. W. M. Peters, F. P. T. Baaijens, and M. Bulters, "Numerical analysis of flow mark surface defects in injection molding flow," *J. Rheol. (N. Y. N. Y).*, vol. 46, no. 3, pp. 651–669, 2002.

[3] G. Wang, G. Zhao, and X. Wang, "Experimental research on the effects of cavity surface temperature on surface appearance properties of the moulded part in rapid heat cycle moulding process," *Int. J. Adv. Manuf. Technol.*, vol. 68, no. 5–8, pp. 1293–1310, 2013.

[4] Y. Donggang, C. Shia-Chung, and H. K. Byung, "Rapid Thermal Cycling of Injection Molds: An Overview on Technical Approaches and Applications," *Adv. Polym. Technol.*, vol. 27, no. 4, pp. 233–255, 2008.

[5] M. Fiorotto, "Mould thermal control for production of weldline-free and high-gloss parts," University of Padua, 2011.

[6] J. Tian *et al.*, "The effects of topology upon fluid-flow and heat-transfer within cellular copper structures," *Int. J. Heat Mass Transf.*, vol. 47, no. 14–16, pp. 3171–3186, 2004.

[7] G. Lucchetta, M. Fiorotto, and P. F. Bariani, "Influence of rapid mold temperature variation on surface topography replication and appearance of injection-molded parts," *CIRP Ann. - Manuf. Technol.*, vol. 61, no. 1, pp. 539–542, 2012.

[8] G. Lucchetta and M. Fiorotto, "Influence of rapid mould temperature variation on the appearance of injection-moulded parts," *J. Mech. Eng.*, vol. 59, no. 11, pp. 683–688, 2013.

[9] L. Crema, M. Sorgato, and G. Lucchetta, "Thermal optimization of deterministic porous mold inserts for rapid heat cycle molding," *Int. J. Heat Mass Transf.*, vol. 109, pp. 462–469, 2017.

[10] EOS GmbH, "Maraging Steel MS1 material datasheet," 2011.